State-Space Approximations of the Orr–Sommerfeld System with Boundary Inputs and Outputs

Arthur C. Or,* Jason L. Speyer,† and John Kim‡
University of California, Los Angeles, Los Angeles, California 90095

Finite-dimensional state-space approximations of the Orr–Sommerfeld equation for plane Poiseuille flow with boundary input and output are discretized to state-space models using two spectral techniques. The models are compared for accuracy and discussed in the context of metrics important for a nonnormal dynamical system. Both state-space models capture the sensitivity behavior of the pole-zero perturbations and the pseudospectrum properties. The effects of balanced truncation ordered by Hankel singular values are discussed. For practical purposes, both methods are effective, and yet certain basic variations in the state-space properties exist. The merits and penalties of the two techniques are also provided.

I. Introduction

DISTRIBUTED-PARAMETERS dynamical systems are described by partial differential equations (PDE) with associated boundary conditions. These systems are solved by numerical discretization to yield sets of ordinary differential equations similar to those in lumped-parameters systems [1,2]. This paper considers the state-space modeling of the two-dimensional (2-D) perturbations of plane Poiseuille flow described by the well-known Orr–Sommerfeld (OS) equation with the incorporation of an input/output structure. Two different spectral techniques are evaluated here. Of interest is existence of some basic variation in the state-space properties consisting of certain nontruncatable superdamped eigenvalues and an input feedthrough term in the output equation. A strong motivation exists to demonstrate the effectiveness of using the finite-dimensional state-space approximations in representing an infinite-dimensional system. The state-space representation is increasingly popular, because numerous toolboxes have been developed based on the state-space form. MATLAB®, for example, offers toolboxes for balancing, model reduction, control design, data analysis, Simulink, and system theory [3]. All require standard state-space representation. For a plane geometry, spectral techniques [4,5] are powerful in constructing state-space models. These are the original models that represent the infinite-dimensional systems. For certain flows, excitable by the input and observable through the output, the original models can be further balanced and order reduced. The balanced reduced-order models (BROMs) are commonly used in designing estimators and controllers.

The OS system is of interest in flow controls, in association with the fundamental problem of transition to turbulence in fluid flows at a much lower Reynolds number than the ones predicted by linear stability theory [6]. For the plane Poiseuille flow, the OS differential operators are highly nonnormal [7,8]. It is well known that, for nonnormal systems, the eigenvalues alone are inadequate to predict the stability of the flow. It can be demonstrated that, even when all eigenmodes are damped, large bursts of transient responses (orders of magnitude greater than the excitations) can be generated for certain transfer functions of a nonnormal system. Although exerting

no exponential growth, these large transient bursts are believed as capable of triggering a transition to turbulence via a subcritical route to instability [6–8].

The aim of this paper is to compare and validate two spectral techniques applied to the OS system and to point out the basic differences between the eigenvalue properties and the state-space representations. A second aim is to demonstrate the sensitivity of the nonnormality of the OS operator [7] and of the transfer function, as well as to show the effects of balanced model truncation.

II. Mathematical Formulation

A. Orr–Sommerfeld System

Consider a plane Poiseuille flow subjected to pumping-and-suction control action (input) at a wall and shear stress measurement at this wall. Both the control action and measured output target the perturbation field. Infinitesimal perturbations are assumed for the streamwise (along the x axis) direction of the flow. The spanwise (y axis) direction has no variation of the perturbations. The perturbation velocity field $\mathbf{v}$ can be described by a complex stream function $\phi(z, t)$. In component form, we have $\mathbf{v} = \nabla \times (-\mathbf{j}\phi) = [u, 0, w]$, with $u = \phi_z(z, t) \exp(ikx)$, $v \equiv 0$, and $w = -ik\phi(z, t) \exp(ikx)$. The cross-stream field (along the z axis) yields the well-known OS system [9]. The PDE system for the OS equation is

$$\mathcal{E}\partial_t\phi(z, t) = \mathcal{L}\phi(z, t); \qquad -ik\phi(-1, t) = u(t)$$
$$\phi_z(-1, t) = 0; \qquad \phi(1, t) = 0; \qquad \phi_z(1, t) = 0 \qquad (1)$$

where $\mathcal{E}$ and $\mathcal{L}$ are, respectively, a second- and fourth-order complex differential operator, defined by

$$\mathcal{E} = \partial_{zz} - k^2; \qquad \mathcal{L} = -ikU(z)\mathcal{E} + ikU_{zz}(z) + \frac{1}{Re}\mathcal{E}^2 \qquad (2)$$

For plane Poiseuille flow, we have $U(z) = 1 - z^2$, and Re is the Reynolds number.

The Fourier component of wall shear stress y provides the output given by

$$y(t) = \mathcal{S}\phi(-1, t) \qquad (3)$$

where $\mathcal{S}$ is a second-order differential operator, defined by $\mathcal{S} = \partial_{zz} + k^2$. Note that the two differential operators $\mathcal{E}$ and $\mathcal{S}$ differ only by a sign.

Both $\mathcal{E}$ and $\mathcal{L}$ can be inverted using appropriate boundary conditions. In the inverted version, we refer to $\mathcal{E}^{-1}\mathcal{L}$ as the OS operator [7,8]. Although this operator has been derived in 2-D in this paper, the Squire's transformation indicates that there is a

*Associate Research Engineer, Mechanical and Aerospace Engineering Department. Senior Member AIAA.
†Professor, Mechanical and Aerospace Engineering Department. Fellow Member AIAA.
‡Professor, Mechanical and Aerospace Engineering Department.

transformation relationship between 2-D perturbations and three-dimensional (3-D) perturbations [9].

B. Spectral Techniques for Discretization

The spectral techniques applied to the infinite-dimensional problem [Eqs. (1–3)] yield a N-order state-space form:

$$\dot{\mathbf{x}} = \mathbf{A}\mathbf{x} + \mathbf{B}u; \qquad y = \mathbf{C}\mathbf{x} + Du \qquad (4)$$

where $\mathbf{x}(t)$ is a $N \times 1$ state vector, $u(t)$ is a complex scalar control action (same notation used for the x component of the perturbation velocity), and $y(t)$ is a complex scalar measurement. Equation (4) describes a complex single-input–single-output system. A compact notation for the N-order state-space approximation is $(\mathbf{A}, \mathbf{B}, \mathbf{C}, D, N)$ or, simply, $(\mathbf{A}, \mathbf{B}, \mathbf{C}, D)$, or $(\mathbf{A}, \mathbf{B}, \mathbf{C})$ if $D \equiv 0$, where $\mathbf{A}$ is referred to as the state matrix, $\mathbf{B}$ is an input vector, and $\mathbf{C}$ is an output vector; D is a scalar feedthrough.

In the following, we describe two well-known spectral techniques to build Eq. (4) from the OS system. A subtlety is in the incorporation of the nonhomogeneous boundary condition involving the control action, $-ik\phi(-1, t) = u(t)$. Both the Galerkin method and the tau method employ the Chebyshev polynomials to form their basis functions. The Chebyshev polynomials form a complete ortho-normal set [4,5]. The basic differences in the two state-space approximations arise in the different ways this boundary condition is being incorporated.

C. Galerkin Method

Individual basis function is picked to satisfy the four homogeneous boundary conditions of Eq. (1) (homogeneous means $u(t) = 0$). To satisfy Eq. (1) with $u(t) \neq 0$, a shape function of choice is prescribed. We pick $\chi(z)$, defined between $-1 \leq z \leq 1$ and satisfied by $\chi(1) = \chi_z(1) = \chi_z(-1) = 0$ and $-ik\chi(-1) = 1$. In a N-order system, the first N-basis functions, expressed in a row vector $\boldsymbol{\varphi}^T(z) = [\varphi_1(z), \varphi_2(z), \ldots, \varphi_N(z)]$ (T denotes the transpose), are used to expand the complex stream field:

$$\phi(z, t) = \boldsymbol{\varphi}^T(z)\mathbf{x}'(t) + \chi(z)u(t) \qquad (5)$$

The incorporation of $\chi(z)$ allows an arbitrary $N \times 1$ vector $\mathbf{x}'$ to satisfy all boundary conditions of $\phi(z, t)$.

Expression (5) yields both $u(t)$ and $\dot{u}(t)$ terms. For the standard state-space models, only $u(t)$ is present. A portion of $\chi(z)u(t)$ can be projected to $\boldsymbol{\varphi}^T$ to be rid of the $\dot{u}$ term. We define a new state vector $\mathbf{x}$, with $\mathbf{x}' = \mathbf{x} - \mathbf{p}u$, where $\mathbf{p}$ is a constant vector to be determined. Substituting Eq. (5) into the PDE and eliminate $\mathbf{x}'$ in favor of $\mathbf{x}$, we have

$$\mathcal{E}\boldsymbol{\varphi}^T\dot{\mathbf{x}} + \mathcal{E}(\chi - \boldsymbol{\varphi}^T\mathbf{p})\dot{u} = \mathcal{L}\boldsymbol{\varphi}^T\mathbf{x} + (\mathcal{L}\chi - \mathcal{L}\boldsymbol{\varphi}^T\mathbf{p})u \qquad (6)$$

A projection of the previous equation to $\boldsymbol{\varphi}(z)$ using the L_2 norm yields:

$$\langle\boldsymbol{\varphi}\mathcal{E}\boldsymbol{\varphi}^T\rangle\dot{\mathbf{x}} + (\langle\boldsymbol{\varphi}\mathcal{E}\chi\rangle - \langle\boldsymbol{\varphi}\mathcal{E}\boldsymbol{\varphi}^T\rangle\mathbf{p})\dot{u} = \langle\boldsymbol{\varphi}\mathcal{L}\boldsymbol{\varphi}^T\rangle\mathbf{x}$$
$$+ (\langle\boldsymbol{\varphi}\mathcal{L}\chi\rangle - \langle\boldsymbol{\varphi}\mathcal{L}\boldsymbol{\varphi}^T\rangle\mathbf{p})u \qquad (7)$$

The matrix integrals for the L_2 norm are denoted by $\langle.\rangle$. If the basis functions are orthonormal, we further have $\langle\boldsymbol{\varphi}(z)\boldsymbol{\varphi}^T(z)\rangle = \mathbf{I}$, an identity matrix. To eliminate the $\dot{u}$ term, we choose $\mathbf{p}$ to satisfy

$$\mathbf{p} = \langle\boldsymbol{\varphi}(z)\mathcal{E}\boldsymbol{\varphi}^T(z)\rangle^{-1}\langle\boldsymbol{\varphi}(z)\mathcal{E}\chi(z)\rangle \qquad (8)$$

It turns out that the choice to eliminate the $\dot{u}$ term in Eq. (7) is more benign than the choice to eliminate the $u(t)$ term, because $\mathcal{E}$ is a second-order operator, whereas $\mathcal{L}$ is fourth order. There is a possibility of a pathological result if $\chi(z)$ is not being picked correctly. Joshi et al. [10,11] used the expression,

$$\chi = \frac{i}{k}\left(\frac{1}{4}z^3 - \frac{3}{4}z + \frac{1}{2}\right) \qquad (9)$$

which works very well [10,11]. With the new state vector, Eq. (7) can be expressed in the standard form, $\dot{\mathbf{x}} = \mathbf{A}_g\mathbf{x} + \mathbf{B}_g u$ (subscript g denotes Galerkin), where

$$\mathbf{A}_g = [\langle\boldsymbol{\varphi}(z)\mathcal{E}\boldsymbol{\varphi}^T(z)\rangle]^{-1}\langle\boldsymbol{\varphi}(z)\mathcal{L}\boldsymbol{\varphi}^T(z)\rangle$$
$$\mathbf{B}_g = [\langle\boldsymbol{\varphi}(z)\mathcal{E}\boldsymbol{\varphi}^T(z)\rangle]^{-1}[\langle\boldsymbol{\varphi}(z)\mathcal{L}\chi(z)\rangle - \langle\boldsymbol{\varphi}(z)\mathcal{L}\boldsymbol{\varphi}^T(z)\rangle\mathbf{p}] \qquad (10)$$

Upon substitution of Eq. (5) in the output Eq. (3), we obtain

$$y(t) = \mathcal{S}\boldsymbol{\varphi}^T(-1)\mathbf{x}'(t) + \mathcal{S}\chi(-1)u(t)$$

After eliminating $\mathbf{x}'$ in favor of $\mathbf{x}$, the standard form of the output equation is $y = \mathbf{C}_g\mathbf{x} + D_g u$, where

$$\mathbf{C}_g = \mathcal{S}\boldsymbol{\varphi}^T(-1); \qquad D_g = \mathcal{S}\chi(-1) - \mathcal{S}\boldsymbol{\varphi}^T(-1)\mathbf{p} \qquad (11)$$

The presence of a nonresidual feedthrough term D_g in the output is an inherent feature of the Galerkin method. Like in the input vector $\mathbf{B}_g$, the feedthrough term depends on $\mathbf{p}$. For a given order N, the Galerkin method yields the state-space approximation denoted by $(\mathbf{A}_g, \mathbf{B}_g, \mathbf{C}_g, D_g, N)$.

The following briefly describes how to obtain the set of basis functions $\varphi_m(z)$ from the Chebyshev polynomials. Following Joshi et al. [10,11], we use the transformation $\boldsymbol{\varphi}^T(z) = \boldsymbol{\beta}'^T(z)\mathbf{G}$, where $\boldsymbol{\beta}'^T(z)$ consists of Chebyshev polynomials,

$$\boldsymbol{\beta}'^T(z) = [T_0(z), T_1(z), \ldots, T_n(z), \ldots, T_{N'}] \qquad (12)$$

where $N' = N + 4$. The N'-by-N $\mathbf{G}$ matrix is tridiagonal. The entries of $\mathbf{G}$ are generated iteratively as

$$\varphi_n(z) = \frac{(n+3)}{(n+1)}T_n(z) - 2\frac{(n+2)}{(n+1)}T_{n+2}(z) + T_{n+4}(z) \qquad (13)$$

for

$$n = 0, 1, 2, \ldots, N$$

where $\{T_n\}$ are Chebyshev polynomials. In this manner, it can be shown that $\{\varphi_n(z)\}$ satisfies all four homogeneous boundary conditions. However, any two basis functions of $\{\varphi_m(z)\}$ are not mutually orthogonal.

D. Tau Method

In the tau method, the boundary conditions are incorporated without resorting to the use of the boundary shape function. The N' Chebyshev polynomials in Eq. (12) are used, with the first N polynomials as basis functions. The last four polynomials provide a tail portion to satisfy the four boundary conditions [12]. Because the Chebyshev polynomials are not all homogeneous, they are allowed to satisfy a nonhomogeneous boundary condition implicitly without resorting to a prescribed shape function. Upon partitioning the basis functions and the tail portion, we denote them by $\boldsymbol{\beta}'^T(z) = [\boldsymbol{\beta}^T(z)\tilde{\boldsymbol{\beta}}^T(z)]$. The tilde quantity denotes the tail portion of the polynomials, which are then eliminated between the dynamical equations with the input and the boundary conditions. To show this process, we let

$$\phi(z, t) = \boldsymbol{\beta}'^T(z)\mathbf{x}'(t) = [\boldsymbol{\beta}^T(z)\tilde{\boldsymbol{\beta}}^T(z)]\begin{bmatrix}\mathbf{x}\\\tilde{\mathbf{x}}\end{bmatrix} = \boldsymbol{\beta}^T(z)\mathbf{x} + \tilde{\boldsymbol{\beta}}^T(z)\tilde{\mathbf{x}} \quad (14)$$

and

$$\partial_t\phi(z, t) = \boldsymbol{\beta}^T(z)\dot{\mathbf{x}} + \tilde{\boldsymbol{\beta}}_1^T(z)\dot{\tilde{\mathbf{x}}}_1$$

where $\tilde{\boldsymbol{\beta}}_1^T(z)$ and $\tilde{\mathbf{x}}_1$ have different lengths than that of $\tilde{\boldsymbol{\beta}}^T(z)$ and $\tilde{\mathbf{x}}$, because the orders of $\mathcal{E}$ and $\mathcal{L}$ are different. The use of variable lengths of tilde vectors is to tailor to the order of the operator being inverted (see McFadden et al. [13]). Substituting the previous expansion into the PDE and projecting with $\boldsymbol{\beta}(z)$, we obtain

$$\langle\boldsymbol{\beta}(z)\mathcal{E}\boldsymbol{\beta}^T(z)\rangle\dot{\mathbf{x}} + \langle\boldsymbol{\beta}(z)\mathcal{E}\tilde{\boldsymbol{\beta}}_1^T(z)\rangle\dot{\tilde{\mathbf{x}}}_1 = \langle\boldsymbol{\beta}(z)\mathcal{L}\boldsymbol{\beta}^T(z)\rangle\mathbf{x}$$
$$+ \langle\boldsymbol{\beta}(z)\mathcal{L}\tilde{\boldsymbol{\beta}}^T(z)\rangle\tilde{\mathbf{x}} \tag{15}$$

The tilde terms $\tilde{\mathbf{x}}$ and $\dot{\tilde{\mathbf{x}}}_1$ are then eliminated in favor of $\mathbf{x}$ by applying the boundary conditions. In a matrix form, the boundary conditions can be stacked to give:

$$\begin{bmatrix} \phi(1) \\ \phi_z(1) \\ \phi(-1) \\ \phi_z(-1) \end{bmatrix} = \begin{bmatrix} \boldsymbol{\beta}'^T(1)\mathbf{x}' \\ \boldsymbol{\beta}_z'^T(1)\mathbf{x}' \\ \boldsymbol{\beta}'^T(-1)\mathbf{x}' \\ \boldsymbol{\beta}_z'^T(-1)\mathbf{x}' \end{bmatrix} = \mathbf{M}'\mathbf{x}' = \begin{bmatrix} \mathbf{M} & \tilde{\mathbf{M}} \end{bmatrix}\begin{bmatrix} \mathbf{x} \\ \tilde{\mathbf{x}} \end{bmatrix}$$

$$= \frac{i}{k}\begin{bmatrix} 0 \\ 0 \\ 1 \\ 0 \end{bmatrix} u(t) \tag{16}$$

Solving for $\tilde{\mathbf{x}}$ in terms of $\mathbf{x}$, we have

$$\tilde{\mathbf{x}} = \tilde{\mathbf{M}}^{-1}(\mathbf{b}u - \mathbf{M}\mathbf{x}) \tag{17}$$

where $\mathbf{b}$ is the 4×1 vector multiplied to $u(t)$ in Eq. (16). A similar boundary relationship can be derived for $\dot{\tilde{\mathbf{x}}}_1$. In this case, the two nonslip boundary conditions are used to invert the $\mathcal{E}$ operator:

$$\dot{\tilde{\mathbf{x}}}_1 = \tilde{\mathbf{M}}_1^{-1}\mathbf{M}\dot{\mathbf{x}} \tag{18}$$

Using Eqs. (17) and (18) to eliminate the tilde terms in Eq. (15), we obtain the N-order dynamical equation with input from the tau method,

$$\dot{\mathbf{x}} = \mathbf{A}_t\mathbf{x} + \mathbf{B}_t u$$
$$\mathbf{A}_t = \mathbf{E}^{-1}[\langle\boldsymbol{\beta}(z)\mathcal{L}\boldsymbol{\beta}^T(z)\rangle - \langle\boldsymbol{\beta}(z)\mathcal{L}\tilde{\boldsymbol{\beta}}^T(z)\rangle\tilde{\mathbf{M}}^{-1}\mathbf{M}]$$
$$\mathbf{B}_t = \mathbf{E}^{-1}\langle\boldsymbol{\beta}(z)\mathcal{L}\tilde{\boldsymbol{\beta}}^T(z)\rangle\tilde{\mathbf{M}}^{-1}\mathbf{b} \tag{19}$$

where

$$\mathbf{E} = \langle\boldsymbol{\beta}(z)\mathcal{E}\boldsymbol{\beta}^T(z)\rangle - \langle\boldsymbol{\beta}(z)\mathcal{E}\tilde{\boldsymbol{\beta}}_1^T(z)\rangle\tilde{\mathbf{M}}_1^{-1}\mathbf{M}_1$$

Unlike the Galerkin method, the nonhomogeneous boundary condition affects both matrices $\mathbf{A}_t$ and $\mathbf{B}_t$, instead of just the input vector. For a prescribed input function $u(t)$, $\boldsymbol{\beta}^T(z)\mathbf{x}(t)$ satisfies all boundary conditions.

The output equation is given by $y(t) = \mathcal{S}\phi(-1, t)$. Upon substitution of the expansion is

$$y(t) = \mathcal{S}\boldsymbol{\beta}^T(-1)\mathbf{x}(t) + \mathcal{S}\tilde{\boldsymbol{\beta}}^T(-1)\tilde{\mathbf{x}}(t)$$

The second term is a residual term that also contains a feedthrough of $u(t)$. However, this feedthrough represents the numerical effect of the truncation error, which converges to zero as $n \to \infty$. A self-consistent truncation scheme gives the standard output equation:

$$y(t) = \mathbf{C}_t\mathbf{x}; \qquad \mathbf{C}_t = \mathcal{S}\boldsymbol{\beta}^T(-1) \tag{20}$$

For given order N, the tau method yields the state-space approximation, denoted here as $(\mathbf{A}_t, \mathbf{B}_t, \mathbf{C}_t)$.

III. Results

A. Complex Versus Real System Representations

Joshi et al. [10,11] and Or and Speyer [14] convert the complex state-space representation to the real representation by increasing the order by a factor of two. The real representation has greater appeal to control analysts. In the real form, all the poles and zeros are in complex conjugate pairs. For frequency responses, one only has to consider one sign of the frequency. For our purpose, a complex representation is used exclusively for the simplicity of a more compact mathematical form. Also, apart from the pole-zero maps, we are interested in the absolute value to the absolute value of the input-to-output relationship, which can be accomplished readily by a complex transfer function.

In Joshi et al. [10,11] and Or and Speyer [14], an N-order complex state-space model, $(\mathbf{A}, \mathbf{B}, \mathbf{C}, \mathbf{D})$, can be converted to a $2N$-order real state-space model, $(\hat{\mathbf{A}}, \hat{\mathbf{B}}, \hat{\mathbf{C}}, \hat{\mathbf{D}})$, by the following conversion,

$$\hat{\mathbf{A}} = \begin{bmatrix} \mathbf{A}_r & -\mathbf{A}_i \\ \mathbf{A}_i & \mathbf{A}_r \end{bmatrix} \tag{21}$$

where $\mathbf{A} = \mathbf{A}_r + i\mathbf{A}_i$; $\mathbf{A}_r$ and $\mathbf{A}_i$ are the real and imaginary parts, respectively. The same conversion is applied to the input and output vectors, as well as the feedthrough term of the complex state-space model. By the Laplace transform, the 2×2 transfer matrix relating the inputs and outputs (both 2×1 vectors) is given by $\hat{\mathbf{y}} = \hat{\mathbf{G}}(s)\hat{\mathbf{u}}$ or, explicitly, by

$$\begin{bmatrix} y_r \\ y_i \end{bmatrix} = \begin{bmatrix} \hat{G}_{11}(s) & \hat{G}_{12}(s) \\ \hat{G}_{21}(s) & \hat{G}_{22}(s) \end{bmatrix}\begin{bmatrix} u_r \\ u_i \end{bmatrix} \tag{22}$$

where $\hat{G}_{ij}(s) = \hat{\mathbf{C}}_i(s\mathbf{I} - \hat{\mathbf{A}})^{-1}\hat{\mathbf{B}}_j$; $i, j = 1, 2$; $\hat{\mathbf{C}}_i$ is the ith row of $\hat{\mathbf{C}}$; and $\hat{\mathbf{B}}_j$ is the jth column of $\hat{\mathbf{B}}$. In Joshi et al. [10], Fig. 1, the pole-zero map is exactly reproduced by converting our complex state-space model (for both Galerkin and tau methods) to the real form using the previous conversion. The outstanding feature is the occurrence of a solitary pole on the right-hand s plane. The pole-zero map in Joshi et al. corresponds to our case with $y_r = \hat{G}_{12}(s)u_i$. This represents exciting the flow by a sine signal, assuming the cosine signal is zero.
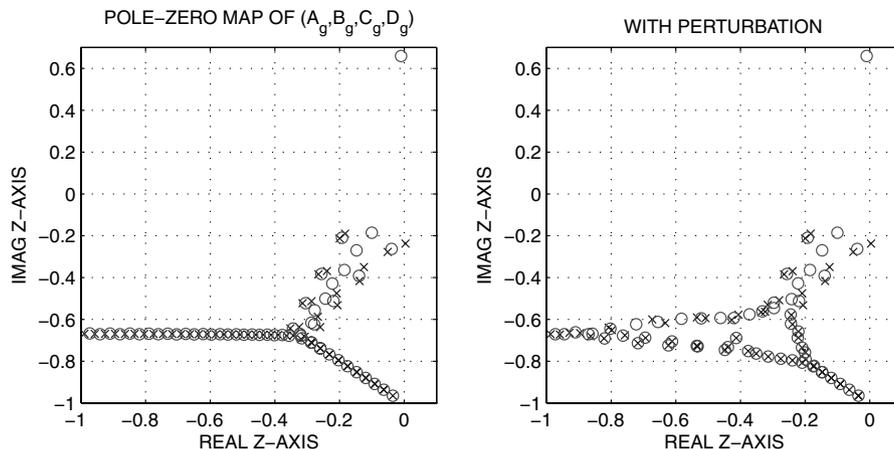

Fig. 1 Pole-zero maps by the Galerkin method.

In a complex notation, we define the complex transfer function $G(z)$, as opposed to the 2×2 Laplace-transformed transfer matrix, by $y_r + iy_i = G(z)(u_r + iu_i)$, where $G(z)$ is defined by $G(z) = \mathbf{C}(z\mathbf{I} - \mathbf{A})^{-1}\mathbf{B}$, where z takes the place of s. Let the complex transfer function be expressed as $G(z) = N(z)/P(z)$. As in the real case, the zeros are defined as the roots of the polynomial $N(z)$, and the poles are the roots of the polynomial $P(z)$. The metrics for nonnormal behavior are conveyed by the absolute values (that is, by $|y_r + iy_i|/|u_r + iu_i| = |G(z)|$). Note that it is not feasible to resolve the transfer functions into real and imaginary parts (that is, $G(z) = G_r(z) + iG_i(z)$), because z is complex.

We report that, in Figs. 1 and 2, there is a zero near $0.0 + 0.6i$, revealed in the pole-zero map using the complex transfer function. This zero is not present in the real representation based on the transfer function of y_r/u_i (see the pole-zero plot in Joshi et al. [10], Fig. 1). The phasing between the outputs and the inputs for the occurrence of this zero is accommodated by the complex transfer function but should be accommodated by the real 2×2 transfer matrix as well. The zeros shown are from the complex transfer function and are also the transmission zero of the real 2×2 transfer matrix; some of these zeros may be shared by the zeros of the individual elements, but not all.

B.   Second-Order Example to Illustrate Nonnormality

We start by using a simple example to illustrate the effect of nonnormality in an operator. Consider a complex second-order system, $(\mathbf{A}, \mathbf{B}, \mathbf{C})$ where $\mathbf{A}$ is complex, given by

$$\mathbf{A} = \begin{bmatrix} \alpha_1 - i\omega_1 & 1 \\ 0 & \alpha_2 - i\omega_2 \end{bmatrix} \tag{23}$$

Consider $\alpha_1 = -0.02$, $\omega_1 = -0.7$, $\alpha_2 = -0.05$, and $\omega_2 = -0.6$. The eigenvalues are $\lambda_1 = -0.02-0.7i$ and $\lambda_2 = -0.05-0.6i$. Both have negative real parts; therefore, any disturbance will decay. However, $\mathbf{A}$ is highly skewed. Consider the resolvent of $\mathbf{A}$ and the transfer function of the second-order system on the complex z plane,

$$\mathbf{R}(z) = (z\mathbf{I} - \mathbf{A})^{-1}; \qquad G(z) = \mathbf{C}\mathbf{R}(z)\mathbf{B} \tag{24}$$

respectively. Note that the absolute value of $\mathbf{R}(z)$ is infinite at exactly either of the two poles. The value of $|G|$ depends on the input and output vectors. Consider two row vectors $\mathbf{e}_1 = [1 \quad 0]$ and $\mathbf{e}_2 = [0 \quad 1]$. We let $z = -0.5i$, reasonably close to the poles. There are four cases: 1) $\mathbf{C} = \mathbf{e}_1$ and $\mathbf{B} = \mathbf{e}_1^T$, $|G| = 50$; 2) $\mathbf{C} = \mathbf{e}_1$ and $\mathbf{B} = \mathbf{e}_2^T$, $|G| = 447$; 3) $\mathbf{C} = \mathbf{e}_2$ and $\mathbf{B} = \mathbf{e}_1^T$, $|G| = 0$; and 4) $\mathbf{C} = \mathbf{e}_2$
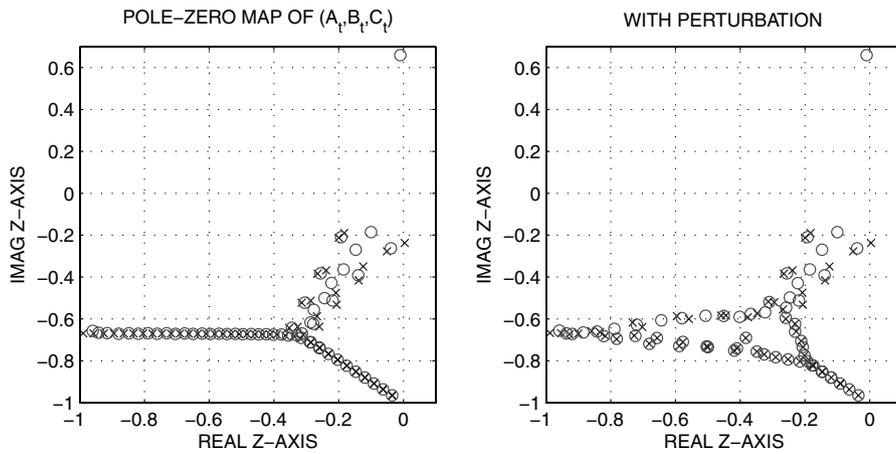

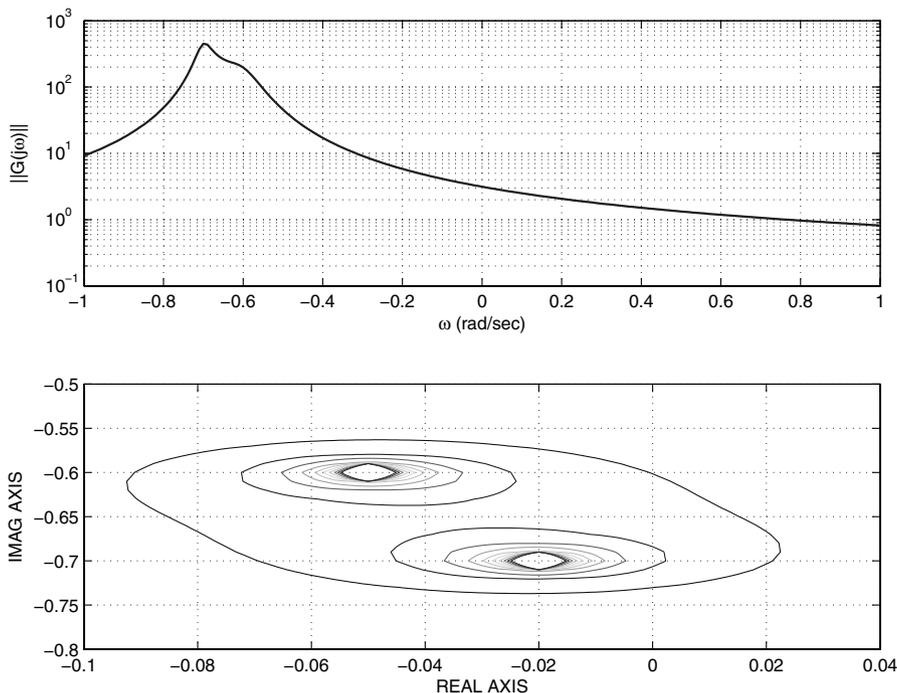Fig. 2   Pole-zero maps by the tau method.

Fig. 3   Spectrum of matrix norm of R (upper panel). Pseudospectrum contours of R (lower panel).

and $\mathbf{B} = \mathbf{e}_2^T$, $|G| = 8.95$. It shows that different choices of input and output vectors produce very different absolute values of the transfer function at a z point. In the second case, it is possible to get two orders of magnitude of amplification. For the third case, the amplification is zero. It implies that $z = -0.5i$ is a zero for this particular pair of input and output vectors.

In the following, we introduce some useful metrics for a nonnormal system. The matrix norm of $\mathbf{R}(z)$ for a given z point is abbreviated as $\|\mathbf{R}(z)\|$, defined as the largest singular value of $\mathbf{R}(z)$. The spectrum of the frequency response of the resolvent norm of the matrix operator $\mathbf{A}$ is defined as $\|\mathbf{R}(i\omega)\|$, where ω represents a range of real frequency (radians per second). Likewise, the spectrum of the frequency response of the transfer function is defined as $|G(i\omega)|$. In the four cases previously stated, the spectrum $|G(i\omega)|$ is evaluated at a single point $\omega = 0.5$. The ϵ pseudospectrum [7,8] of the resolvent norm of $\mathbf{A}$ is defined as a region in the complex z plane (possibly nested) by $\{z \in \mathcal{C}: \|\mathbf{R}(z)\| \geq \epsilon^{-1}\}$.

In Fig. 3, we show the spectrum $\|\mathbf{R}(i\omega)\|$ (upper panel). Unlike a normal matrix, a nonnormal matrix (as shown in Fig. 3 upper panel) has a broad peak spectrum. Because of the broadband, it is also helpful to show the pseudospectrum. In Fig. 3, the lower panel shows the ϵ pseudospectrum contours in ϵ^{-1} increments of 200, from 0 to 2000. The largest contour line, including all the others at smaller ϵ values, corresponds to $\epsilon^{-1} = 200$. In summary, the metrics of a highly skewed second-order matrix operator is sufficient to illustrate the large transient behavior and demonstrates the insufficiency of using eigenvalues alone for predicting stability.

C. Orr–Sommerfeld System: Pole-Zero Maps, Spectra, and Pseudospectra

For the OS system, the transfer functions obtained using the Galerkin method and the tau method are, respectively, $G_g(i\omega)$ and $G_t(i\omega)$. They are given by $G_g(i\omega) = \mathbf{C}_g\mathbf{R}_g(i\omega)\mathbf{B}_g + D_g$ and by $G_t(i\omega) = \mathbf{C}_t\mathbf{R}_t(i\omega)\mathbf{B}_t$, where the resolvents are defined by $\mathbf{R}_g(i\omega) = (i\omega\mathbf{I} - \mathbf{A}_g)^{-1}$ and $\mathbf{R}_t(i\omega) = (i\omega\mathbf{I} - \mathbf{A}_t)^{-1}$.

The pole-zero map provides the fingerprint for the transfer function. The poles are the complex roots of the polynomial of the denominator, which are the eigenvalues. Therefore, the poles depend only on the state matrix. The zeros are the complex roots of the polynomial of the numerator, which depend not only on the dynamics but on the input/output relationship as well.

We consider $k = 1$ and $Re = 10^4$. This case is considered by several authors [7,10,14]. In this case, the flow is weakly unstable according to the eigenvalue analysis. This case is good to demonstrate the strong effects of the large transient bursts due to the nonnormality of the OS operator. Figures 1 and 2 show the pole-zero maps for $G_g(z)$ and $G_t(z)$, respectively. The poles are marked by ×, and the zeros are marked by o. The original pole-zero maps are shown in the left panels of the figures. On the scale shown, the agreement between the two methods is very good. Worth noting is the pole located near the imaginary axis in the right-hand plane, which makes the system unstable. A zero that appears near $z = 0.0 + 0.6i$ is responsible for the dip in the transfer function spectrum. On the extended scale, the two methods start to show significant deviations with respect to the fast poles and zeros. In particular, the tau method possesses a pair of superdamped poles that are not present in the Galerkin method. In the left panels, the three branches of poles, discussed extensively by Reddy et al. [7], are recaptured here. The horizontal and lower branches have the poles, and the zeros closely alternate or overlap. An overlap between a pole and a zero indicates a pole-zero cancellation. When it happens, the eigenmode in the dynamics characterized by this pole is either uncontrollable or unobservable by the choice of the input/output. For pole-zero pairs that nearly overlap, the dynamics are weakly controllable or observable. Upon balancing, these modes correspond to small Hankel singular values (HSVs) and are likely to be truncated in the BROMs.

Of interest is to see whether the Galerkin and the tau methods are capable of capturing the pole sensitivity discussed in detail by Reddy et al. [7]. The authors reported their observation of the sensitivity near the branch point of the three branches of poles to noises added to the OS operator. To show this sensitivity, instead of adding a small random number to every entry of the state matrix, we add it only to the diagonal entries. Small zero-mean Gaussian random numbers (with known seed for repeatability) with a standard deviation of 10^{-6} are used for $\mathbf{A}_g$ and then with the same random numbers for $\mathbf{A}_t$. For one set of random numbers, the results are shown on the right panels of Figures 1 and 2. The sensitivity of the eigenvalues to the noises is indicated by the poles. However, in the pole-zero maps, we also observe that the zeros associated with the sensitive poles move with the poles as well. As the sensitive pole-zero pairs are perturbed, they move but remain almost-cancelled pairs.

Next, we perform a comparison between the two methods, using the frequency responses of the resolvent norms and the transfer
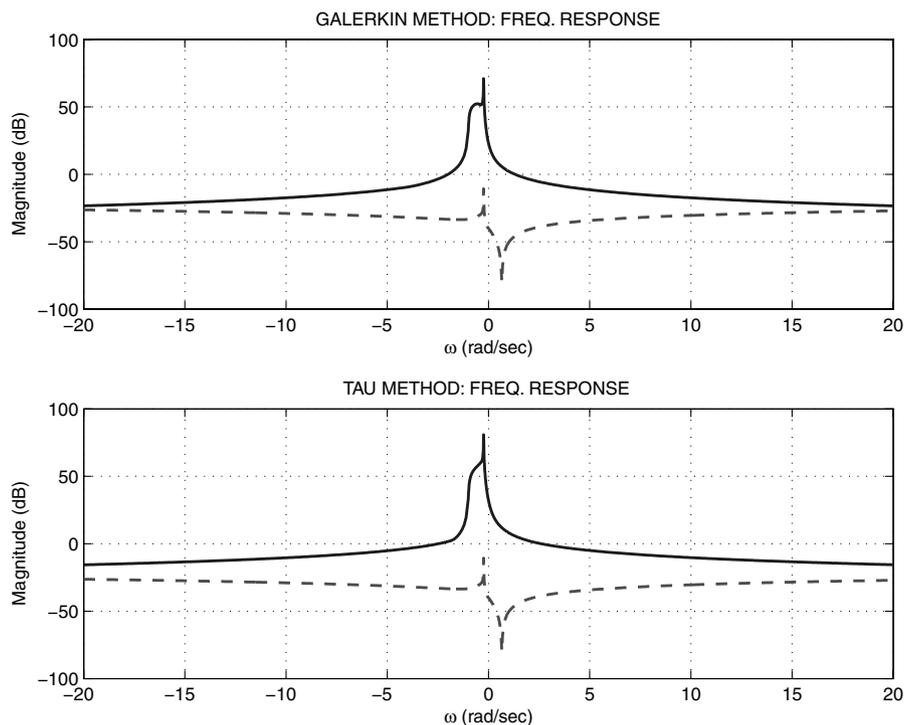

Fig. 4   Frequency responses by the Galerkin method (upper panel) and by the tau method (lower panel).

functions, for a range of frequency of interest ω (radian per second). The results are shown in Fig. 4. Instead of separating the complex state-space model into a real form, we keep the complex model but consider both negative and positive frequencies. The results are easier to interpret with the complex form than with the real form. For the Galerkin method (upper panel) the solid line corresponds to the norm of the resolvent, $20\log_{10}[\|\mathbf{R}_g(i\omega)\|]$ (in dB), and the dashed line corresponds to the gain of the transfer function, $20\log_{10}\|G_g(i\omega)\|$ (in dB). Similarly, for the tau method (lower panel), we have $20\log_{10}[\|\mathbf{R}_t(i\omega)\|]$ (solid line) and $20\log_{10}\|G_t(i\omega)\|$ (dashed line).

The magnitudes of the resolvent norm and the transfer function differ by roughly $\mathcal{O}(Re^{-1})$, a factor that occurs in the output equation. In Fig. 4, the maximum of the resolvent norm is about 1.1×10^4, and the maximum of the transfer function is about 0.29. The peaks of the resolvent norm and the transfer function occur at about $\omega = -0.25$. The resolvent norm of the OS operator shows a broadband peak, which is characteristic of the highly nonnormal operator. However, the transfer function shows a very narrow peak. The narrow peak in the transfer function suggests that the input and the output weaken the nonnormality effects. In other words, the modes of disturbances that are responsible for the dramatic transient amplification in the nonnormal OS operator are not excited or observable by our input and output transfer function. There is a dip in the transfer function, or zero, at about $\omega = 0.65$. At this frequency, regardless of the wall pumping-and-suction input, the disturbance wall shear stress output diminishes. The agreement between the two frequency responses [i.e., the Galerkin method (upper panel) and the tau method (lower panel)] remains very good.

Another comparison between the Galerkin method and the tau method is performed, respectively, using the ϵ pseudospectrum contour plots of the resolvents $\mathbf{R}_g(z)$ and $\mathbf{R}_t(z)$. In Fig. 5, the results from the Galerkin method (left panel) and the tau method (right panel) are shown side by side. The contours have equal increments of $10^{0.2}$, from a value of 10^2 (outermost line) to 10^6 (innermost line). Both panels show very similar results, except for the tau method, the upper-left corner of the panel shows a bigger bump. The salient feature is the extremely high resolvent norm toward the lower triangular-shaped region. This region coincides with the region in which high sensitivity in the pole-zero pairs exist (see Figs. 1 and 2, right panels).

Reddy et al. [7] and Trefethen et al. [8] point out that the large-burst transient disturbance pertains to 3-D rather than 2-D. As pointed out by the authors, the traditional emphasis of stability analysis is to capture the first pole crossing to the right side of the z plane by increasing the Reynolds number. This view is greatly influenced by Squire's theorem [9], which states that for any given 3-D disturbance field corresponding to a certain Reynolds number, there always exists a 2-D disturbance field at a lower Reynolds number that satisfies the Squire-transformed equations. In the view of highly skewed dynamical systems, what matters for instability is the ability of the systems to excite (and observe) large transient responses. Such responses can occur before the emergence of the first bifurcation (i.e., when all the poles have negative real parts).

D.   Balanced Reduced-Order Models

For the N-order controllable and observable state-space system, the controllability Gramian $\mathbf{W}_c$ and the observability Gramian $\mathbf{W}_o$ can both be diagonalized by a similarity transformation $\mathbf{T}$, such that

$$\mathbf{T}^{-1}\mathbf{W}_c(\mathbf{T}^{-1})^+ = \mathbf{T}^+\mathbf{W}_o\mathbf{T} = \boldsymbol{\Sigma} \qquad (25)$$

This process is called a balanced realization. The N entries of $\boldsymbol{\Sigma}$ are ordered in descending values, called HSVs. The HSVs provide a metric for ordering the modes according to the energy content of the modes being excitable and observable. Let us form a projection pair from the first N_r ($N_r < N$) rows of $\mathbf{T}^{-1}$, denoted as $\mathbf{S}_1$, and from the first N_r columns of $\mathbf{T}$, denoted as $\mathbf{T}_1$. This projection is called balanced truncation. The balanced reduced-order state-space model (BROM) for the Galerkin method is $(\mathbf{S}_1\mathbf{A}_g\mathbf{T}_1, \mathbf{S}_1\mathbf{B}_g, \mathbf{C}_g\mathbf{T}_1, D_g)$. The balance realization can be adequately performed using the standard MATLAB script. We refer readers to Laub et al. [15] for the theory of the transformations that simultaneously diagonalizes the Gramians. For the tau method, similar balanced realization and truncation are performed.

For both Galerkin and tau methods, the N-order balanced realizations are obtained. The balanced N-order systems are fully controllable and observable and have the same properties as the original systems, as shown in Figs. 1, 2, 4, and 5. It is of interest to see how balanced truncation is effected when a large number of states corresponding to lower HSVs are truncated. In the following, we compare the pole-zero maps, the frequency responses, and the pseudospectra obtained from the BROMs of the Galerkin and the tau methods. For illustration purpose, we consider $N_r = 20$, even though certain metrics remain unchanged for even lower N_r.

The BROMs by the Galerkin method and the tau method agree well. The pole-zero map comparison is presented in Fig. 6. The balance truncation has an effect of shifting the locations of some poles and zeros. However, the highly controllable and observable ones are unchanged. For example, the unstable pole and the zero in the upper region are not moved. The state matrix operator of the BROMs no longer exhibits sensitivity to noises. We conclude that the sensitive pole-zero pairs are associated with weak controllability and observability. In Fig. 7, we show the frequency responses. Again, the agreement between the Galerkin and the tau methods is good. The peak of the resolvent norm of the state matrix in BROMs is roughly an order of magnitude weaker than that of the original model. In contrast, for the frequency responses of the transfer functions, the BROMs agree well with that of the original models. The results suggest that the BROMs approximate the original models well for the transfer function but not the resolvent norm of the state matrix operator. The balanced truncation weakens the effects of non-normality significantly. The conclusion is that a lot of weakly controllable and observable modes are important for the nonnormal skewness of the OS operator. These modes are filtered off for the input/output structure. So far, we use 20 balanced modes in the BROMs. In fact, we only have to keep the first five balanced modes in
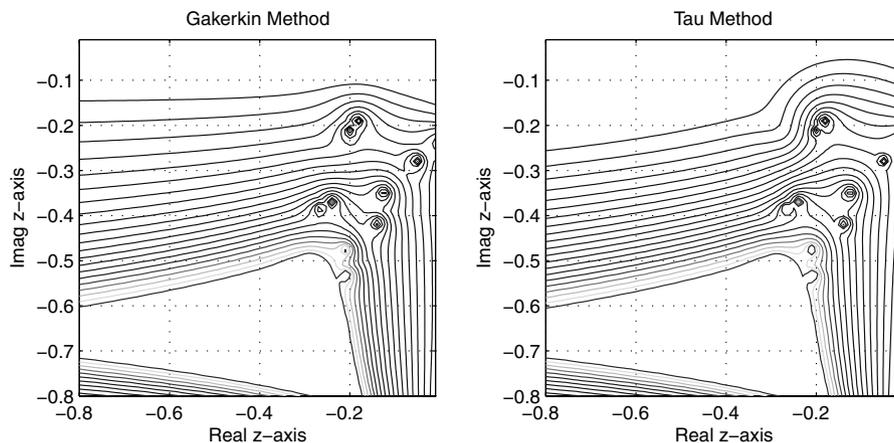

Fig. 5 ϵ Pseudospectra of $\|\mathbf{R}(z)\|$ for the Galerkin method (left panel) and for the tau method (right panel).
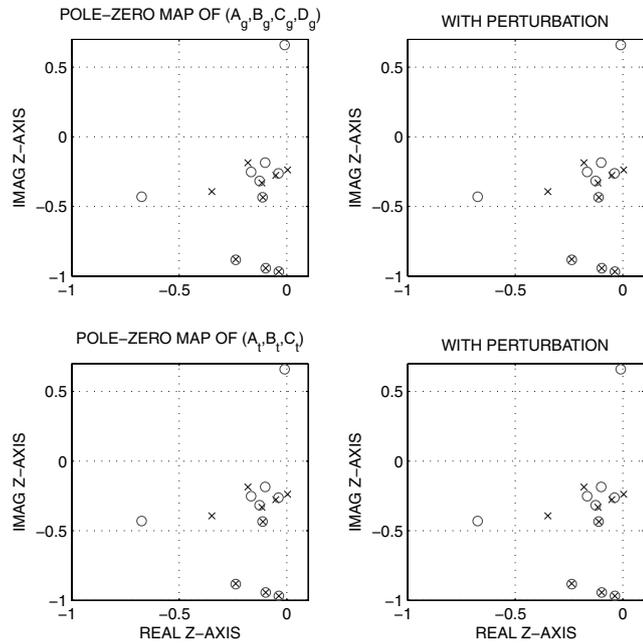
Fig. 6 BROM: Pole-zero maps with perturbation (right panels) and without perturbation (left panels).

order for the transfer function spectra to agree between the BROMs and the original models.

Lastly, the BROM version of the ϵ-pseudospectrum contour plot for the resolvent is compared between the Galerkin and tau methods in Fig. 8. In this case, due to the smaller magnitude of the pseudospectra, the same contour increments apply with a factor of $1/20$. Compared with Fig. 5, we observe that the contour shapes are very different. The triangular region of sensitivity is no longer present. The BROMs do not preserve the ϵ pseudospectra.

E. Super-Damped Eigenvalues and Feedthrough

The Galerkin method yields a nonresidual, imaginary feedthrough term D_g. By contrast, the feedthrough term from the tau method is a

residual from numerical truncation, which is ignored. Less obviously, in the tau method, there is a pair of fast poles that show up in the very far left of the real axis of the complex z plane, with approximate values of -4.8×10^7 and -8.06×10^7. Their magnitudes are too large to be captured in the pole-zero maps. After performing the balanced model reduction, both poles are still in the BROM. This pair of fast poles is intrinsic to the tau method to represent the nonhomogeneous boundary condition. If they are truncated away, the state-space model will fall apart. In the tau method representation, the most large-scale mode of interest is associated with a small tilde portion, which accounts for the truncation error. For this pair of superdamped poles, their tilde portions are not small. It is not hard to see that the nonhomogeneous eigenfunctions associated with the superdamped poles play a similar role as the shape function $\chi(z)$ in the Galerkin method.

There is a simple way to demonstrate the convertibility between the two state-space approximations. Denote $(\Lambda_t, \hat{\mathbf{B}}_t, \hat{\mathbf{C}}_t)$ as the eigenvalue-decomposed N-order state-space system by the tau method. The ith component equation is given by $\dot{a}_{ti} = \lambda_{ti} a_{ti} + \hat{B}_{ti} u$ $(i = 1, 2, \ldots, N)$. In closed form, the modal amplitude is

$$a_{ti}(t) = \exp(\lambda_{ti} t) a_{ti}(0) + \hat{B}_{ti} \int_0^t \exp \lambda_{ti}(t - \tau) u(\tau) \, d\tau$$
$$i = 1, 2, \ldots, N \tag{26}$$

The two input coefficients corresponding to the superdamped poles have approximate imaginary values of $-2.4 \times 10^7 i$ and $3.4 \times 10^7 i$, on the same order of magnitude as these poles. From Eq. (26), the first term on the right-hand side is vanishingly small. The second term can be evaluated if $u(t)$ is given. For a unit-step input signal, for example, $a_{ti} \rightarrow -\hat{B}_{ti}/\lambda_{ti}$ (where $i = N - 1, N$ for the pair of poles) and have $\mathcal{O}(1)$ values.

By eliminating the two superdamped poles (not truncating), the remaining $(N - 2)$-order state-space approximation resembles the N-order Galerkin state-space approximation. This is done by substituting the two a_{tj} terms given in Eq. (26) into the output equation:

$$y(t) = [\hat{C}_1, \ldots, \hat{C}_{N-2}] \begin{bmatrix} a_1 \\ \vdots \\ a_{N-2} \end{bmatrix} + D_t u(t) \tag{27}$$
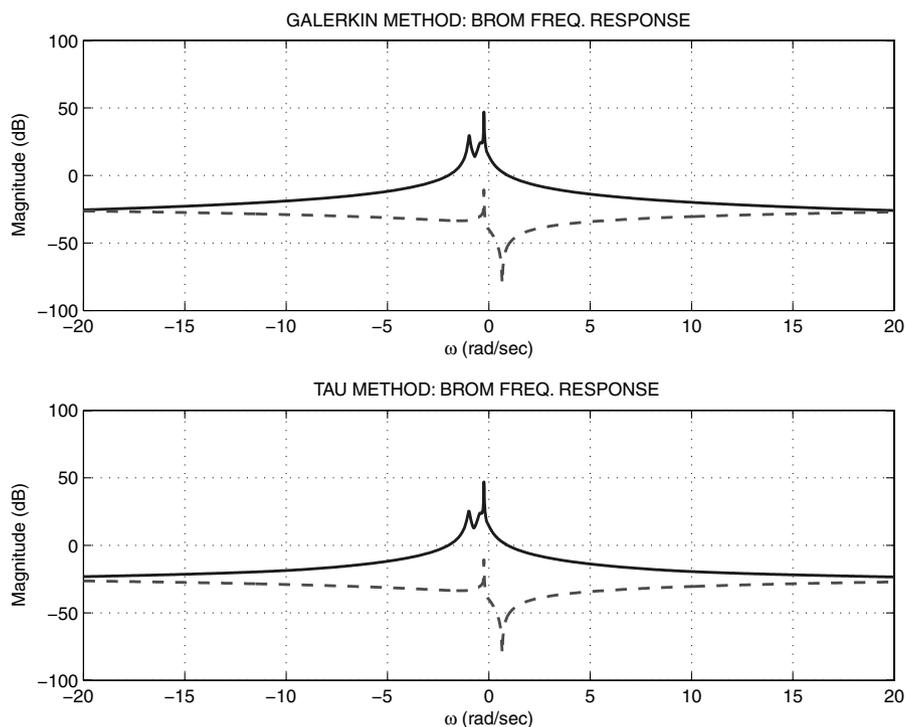

Fig. 7 BROM: Frequency responses by the Galerkin method (upper panel) and by the tau method (lower panel).
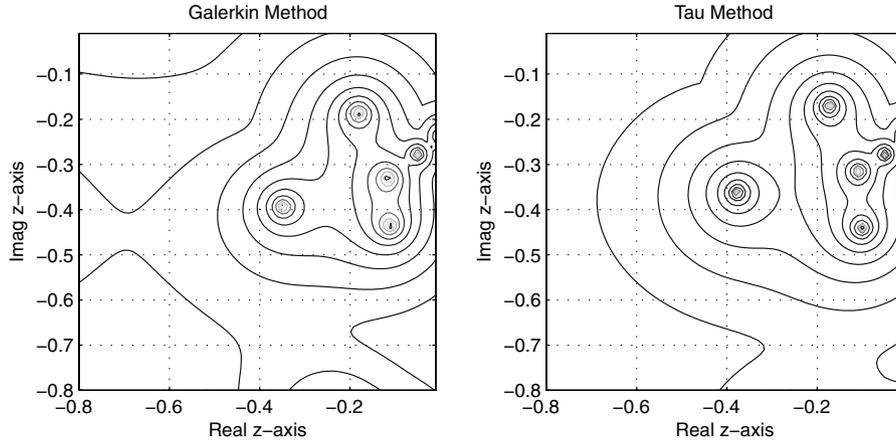
Fig. 8   BROM: Pseudospectra of $\|R(z)\|$ for the Galerkin method (left panel) and the tau method (right panel).
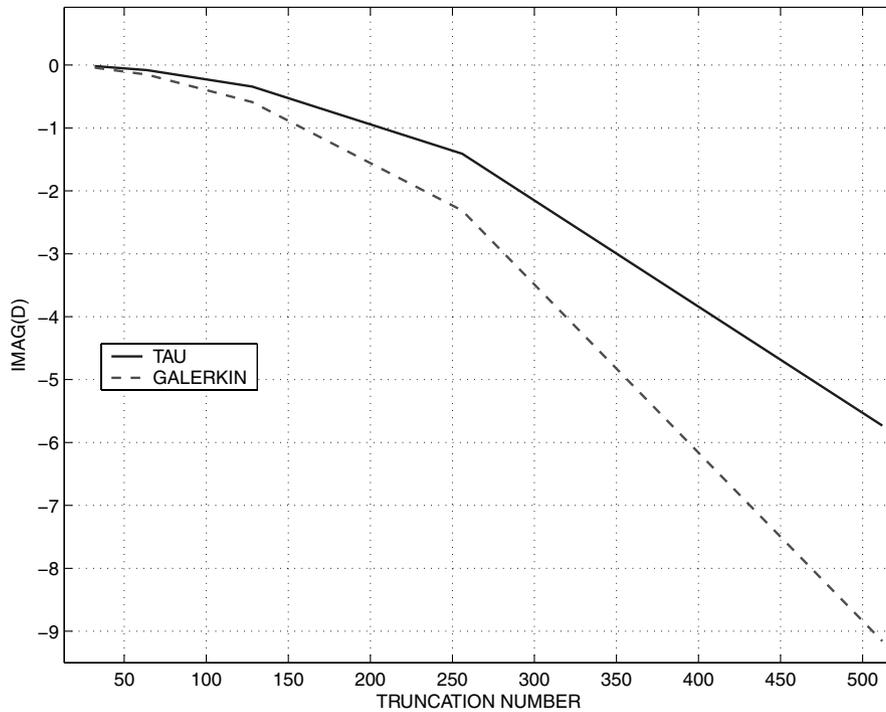

Fig. 9   Feedthrough term versus truncation number.

In the process of elimination, a feedthrough term is generated:

$$D_t = -(\hat{C}_{N-1}\hat{B}_{N-1}/\lambda_{N-1} + \hat{C}_N\hat{B}_N/\lambda_N) \qquad (28)$$

In Fig. 9, we compare the feedthrough term D_t, obtained from Eq. (28), with the feedthrough term D_g of the Galerkin method [see Eq. (11)]. We plot them for different truncation numbers. Both feedthrough terms are purely imaginary [see Eq. (5) and the boundary condition $-ik\phi(-1, t) = u(t)$]. The solid line represents D_t, and the dashed line represents D_g. The result shows good qualitative agreement but not quantitative agreement. We remark that the elimination process is not exact unless the superdamped poles approach infinity.

IV.   Conclusions

Both the Galerkin and tau methods yield accurate finite-order state-space approximations for the OS system, incorporated with wall pumping-and-suction control input and wall shear measurement output. The metrics used for testing the state-space approximations include the spectra and pseudospectra of the resolvent of the OS operator and the spectra of the transfer function. The basic

differences and convertibility between the two state-space approximations are highlighted. As far as merits and shortcomings, the nontruncatable superdamped eigenvalues in the tau method make the system stiffer; as a result, semi-implicit numerical integration schemes have to be used. However, the tau method is simpler for implementation, because it uses the Chebyshev polynomials directly as basis functions. The boundary conditions are easier than the Galerkin method to implement. The absence of a feedthrough term is a desirable feature.

The sensitivity of the poles around where the three branches of poles meet is captured in the state-space approximations. For our input/output configuration, a lot of these sensitive poles overlapped with corresponding zeros. When the OS operator is perturbed by noises, these sensitive poles and zeros move but remain basically cancelled pairs. These sensitive poles are responsible for the broad and prominent peak structure in the resolvent norm of the operator. However, they are weakly controllable or observable to the input and output. These sensitive pole-zero pairs are not in the BROMs. It explains why the BROM state matrices are not strongly skewed. On the other hand, the transfer function between the original state-space models and the BROMs agree with one another reasonably well.

Acknowledgments

References

[1] Curtin, R. F., and Swart, H. J., *An Introduction to Infinite-Dimensional Linear Systems*, Springer–Verlag, New York, 1995.

[2] Bensoussan, A., Da Prato, G., Delfour, M. C., and Mitter, S. K., *Representation and Control of Infinite Dimensional Systems*, 2nd ed., Birkhauser, Boston, 2007.

[3] Chen, C. T., *Linear System Theory and Design*, Oxford Series in Electrical and Computer Engineering, Oxford Univ. Press, Oxford, 1998.

[4] Canuto, C., Hussaini, M. Y., Quarteroni, A., and Zang, T. A., *Spectral Methods in Fluid Dynamics*, Springer Series in Computational Physics, Springer–Verlag, New York, 1986.

[5] Gottlieb, D., and Orszag, S. A., *Numerical Analysis of Spectral Methods: Theory and Applications*, Society for Industrial Mathematics, Philadelphia, 1981.

[6] Orszag, S. A., and Patera, A. T., "Secondary Instability of Wall-Bounded Shear Flows," *Journal of Fluid Mechanics*, Vol. 128, No. -1, 1983, pp. 347–385.
doi:10.1017/S0022112083000518

[7] Reddy, S. C., Schmid, P. J., and Henningson, D. S., "Pseudospectra of the Orr–Sommerfeld Operator," *SIAM Journal on Applied Mathematics*, Vol. 53, No. 1, Feb. 1993, pp. 15–47.

doi:10.1137/0153002

[8] Trefethen, L. N., Trefethen, A. E., Teddy, S. C., and Driscoll, T. A., "Hydrodynamics Stability Without Eigenvalues," *Science*, Vol. 261, No. 5121, 1993, pp. 578–584.
doi:10.1126/science.261.5121.578

[9] Drazin, P. G., and Reid, W. H., *Hydrodynamic Stability*, Cambridge Univ. Press, New York, 1982.

[10] Joshi, S. S., Speyer, J. L., and Kim, J., "A Systems Theory Approach to the Feedback Stabilization of Infinitesimal and Finite-Amplitude Disturbances in Plane Poiseuille Flow," *Journal of Fluid Mechanics*, Vol. 332, 1997, pp. 157–184.

[11] Joshi, S. S., Speyer, J. L., and Kim, J., "Finite-Dimensional Optimal Control of Poiseuille Flow," *Journal of Guidance, Control, and Dynamics*, Vol. 22, No. 2, 1999, pp. 340–348.
doi:10.2514/2.4383

[12] Lanczos, C., *Applied Analysis*, Prentice–Hall, Englewood Cliffs, NJ, 1956.

[13] McFadden, G. B., Murray, B. T., and Boisvert, R. F., "Elimination of Spurious Eigenvalues in the Chebyshev Tau Spectral Method," *Journal of Computational Physics*, Vol. 91, No. 1, 1990, pp. 228–239.
doi:10.1016/0021-9991(90)90012-P

[14] Or, A. C., and Speyer, J. L., "Model Reduction of Input–Output Dynamical Systems by Proper Orthogonal Decomposition," *Journal of Guidance, Control, and Dynamics*, Vol. 31, No. 2, 2008, pp. 322–328.
doi:10.2514/1.29456

[15] Laub, A. J., Heath, M. T., Paige, C. C., and Ward, R. C., "Computation of System Balancing Transformations and Other Applications of Simultaneous Diagonalization Algorithms," *IEEE Transactions on Automatic Control*, Vol. 32, No. 2, 1987, pp. 115–122.
doi:10.1109/TAC.1987.1104549